25th ABCM International Congress of Mechanical Engineering
October 20-25, 2019, Uberlândia, MG, Brazil

COB-2019-0775
PATTERN FORMATION SURVEY ON NON UNIFORMLY FORCED SWIFT-HOHENBERG EQUATION

Daniel Coelho
José Pontes
Norberto Mangiavachi
State University of Rio de Janeiro - UERJ, R. Fonseca Teles 121, 20940-903, Rio de Janeiro, Brazil
danielcoelho.uerj@gmail.com, pontes@uerj.br, norberto.mangiavacchi@gmail.com

Abstract. *The present paper considers a generalized nonlinear diffusion equation known as the Swift-Hohenberg (SH) equation. Applications of this equation include the study of pattern formation in physical problems outside equilibrium, described by phase field models, such as the hydrodynamic instability of a fluid under thermal convection or even the structural evolution of nanostructured copolymers. Numerical solutions of the SH equation present patterns with a large number of topological defects, e.g., grain boundaries, dislocations and disclinations ; so computational modelling of such mesoscopic characteristics can help us to understand, explain and predict macroscopic properties of an extended system of interest. A finite-difference semi-implicit time splitting scheme is employed on the discretization of the governing equation in two dimensions. Simulations were performed with nonuniform forcings such as ramped and gaussian distributions. Bidimensional rolls patterns (stripes) were obtained from random initial conditions and numerical stability is verified. Distinct structure orientation and a subcritical effect can be observed for miscellaneous domain sizes and forcings.*

Keywords : *Swift-Hohenberg Equation, Pattern Formation, Topological Defects, Implicit Methods, Finite Difference Methods*

1. INTRODUCTION

A widely accepted model for describing pattern formation in a thin layer of fluid heated from below is the so-called Swift-Hohenberg (SH) equation (Swift and Hohenberg, 1977), which is a nonlinear parabolic equation containing fourth-order space-derivatives (generalized diffusion equation). The equation first appeared in the framework of Bénard thermal convection between two "infinite" horizontal surfaces with temperatures T_0 and $T_0 + \Delta T$, confined between horizontal well-conducting boundaries. When the Rayleigh number R, which is a dimensionless temperature difference ΔT, is larger than a critical value R_c, a structure of convective rolls emerges and can be seen from the top view of the x-y plane. A scheme of the convection cell is shown in Fig. 1 :

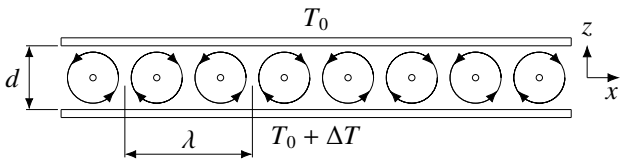

FIGURE 1. A scheme of a Rayleigh-Bénard convection cell.

Though frequently used to model pattern formation in a wide class of systems, not many studies are found in the literature, addressing the problem with a nonuniform control parameter across the domain (Walton, 1982, 1983).

Understanding the selection and orientation mechanisms of the spatial structures, their symmetries and instabilities represent a major theme of theoretical and experimental research in mathematical modelling and numerical simulation of self-organization phenomena. Spatio-temporal organization is nowadays recognized to be related to several technological problems in physics, chemistry, nonlinear optics, and materials science. Tin this last case, the long-term goal is to apply such modelling and numerical results to large scale systems in order to achieve predictive capabilities regarding computational materials science (Walgraef, 1997).

Following Christov *et al.* (1997),Christov and Pontes (2002), we solve the SH equation in the nodes of a structured and staggered grid of points uniformly spaced, in square domains. Spatial derivative operators are represented by second order finite difference formulæ and time discretization is made with a second order Crank-Nicolson scheme. Furthermore, we employ the Douglas second scheme (Douglas and Rachford., 1956; Yanenko and Holt, 1971), also known as the stabilizing correction scheme, to construct an efficient splitting scheme for solving the equation. This is the numerical objective of

the present paper. The second objective was to attain physically relevant results by examing structure behaviour in the presence of a nonuniform control parameter (ϵ in the form of ramped and Gaussian distributions.)

2. MATHEMATICAL MODELLING AND NUMERICAL SCHEME

2.1 Governing equation

The Swift-hohenberg equation has the so-called gradient dynamics, which means there is a potential, known as a Lyapunov functional, associated with the order parameter field $\psi(x, y, t)$ that has the property of decreasing monotonically during the dynamics. This non-increasing behaviour of the Lyapunov functional $\mathcal{F}$ for the SH equation is clearly demonstrated by Christov and Pontes (2002). Adopting the following time-dependent Ginzburg–Landau equation with conserved dynamics for the order parameter $\psi(x, y, t)$ and neglecting the advection term, we have :

$$\frac{\partial \psi}{\partial t} = -\frac{\delta \mathcal{F}}{\delta \psi} \tag{1}$$

Discussions about this model equation applied to block copolymers dynamics is performed by Viñals (2009). Then, for example, a block copolymer melt can be described by a simpler coarse-grained free energy (the Brazovskii or Leibler energy), shown by Viñals (2009)) :

$$\mathcal{F}[\psi] = \int_D d\mathbf{r} \left\{ -\frac{1}{2}\epsilon\psi^2 + \frac{1}{2}\left[(k_0^2 + \nabla^2)\psi\right]^2 - \frac{1}{3}g_1\psi^3 + \frac{1}{4}\psi^4 \right\} \tag{2}$$

Where D represents the domain whose size commensurate with the length scales of the patterns. We considered a rectangle $x \in [0, L_x]$, $y \in [0, L_y]$ and generalized Dirichlet boundary conditions (GDBC), $\psi = \partial\psi/\partial n = 0$, where n stands for the outward normal direction to the boundary. Periodic boundary conditions (PBC) were used as well.

The dimensionless parameter ϵ is the control parameter, which represents the distance to threshold (how close R is to the critical value R_c) in the form $\epsilon = (R - R_c)/R_c$ (assuming $R_c \neq 0$), e.g., in the case of Rayleigh-Bénard convection. This control parameter assumes the following range of values in the present framework : $-0.2 \leq \epsilon \leq 0.2$. The onset of linear instability $R = R_c$ is represented by $\epsilon = 0$.

The parameter g_1 is associated to symmetry breaking, leading to hexagonal structures that will not be addressed here and thus : $g_1 = 0$. However, in general, the quadratic nonlinearity plays an important role regarding reaction-diffusion systems (e.g., the brusselator). In those kind of systems, species interactions take the form of nonlinear terms and its linear stability analysis may reveal instability points dependent of the equation parameters. Near those points, the time and space scale associated to the unstable modes increase and tend to infinity at the bifurcation, leading to critical slowing down phenomena. Hence the unstable modes evolve on much longer time scales than the stable ones which may be adiabatically eliminated from the asymptotic dynamics. The expansion of the stable mode amplitude as a series of powers of the unstable mode amplitude can be performed and is restricted to the weakly nonlinear regime around the instability point to the first significant nonlinearities, leading to asymptotic dynamics of the Ginzburg-Landau type where the unstable modes play the role of the order parameter. The reduction to the unstable modes dynamics by this method was performed by Haken (1983, 1993) and Walgraef (1997) for several physical problems, including reaction-diffusion mechanisms in physics, chemistry and materials science.

In the case of Rayleigh-Bénard instability for a Boussinesq fluid (Pontes and Mangiavacchi, 2016; Pontes *et al.*, 2018), Swift and Hohenberg performed this reduction, which leads to the following evolution equation for convective patterns (Swift and Hohenberg, 1977). Considering all quantities to be dimensionless, we have the so-called Swift-Hohenberg equation :

$$\frac{\partial \psi}{\partial t} = \epsilon\psi - (k_0^2 + \nabla^2)^2\psi + g_1\psi^2 - \psi^3 \tag{3}$$

which can also be obtained by substituting Eq. (2) in the Ginzburg-Landau equation (1). Developing the term $(k_0^2 + \nabla^2)^2\psi$, we have :

$$\begin{aligned} \frac{\partial \psi}{\partial t} &= \epsilon\psi - k_0^4\psi - 2k_0^2\nabla^2\psi - \nabla^4\psi + g_1\psi^2 - \psi^3 \\ &= \epsilon\psi - k_0^4\psi - 2k_0^2\frac{\partial^2\psi}{\partial x^2} - 2k_0^2\frac{\partial^2\psi}{\partial y^2} - \frac{\partial^4\psi}{\partial x^4} - 2\frac{\partial^4\psi}{\partial x^2 y^2} - \frac{\partial^4\psi}{\partial y^4} + g_1\psi^2 - \psi^3 \end{aligned} \tag{4}$$

Where the laplacian operator is given by : $\nabla^2 \equiv \partial^2/\partial x^2 + \partial^2/\partial y^2$. The present work consisted of integrating the nonuniformly forced SH equation without the quadratic nonlinearity ($g_1 = 0$) by the finite differences method. The following second order in time Crank-Nicolson semi-implicit scheme was adopted :

$$\frac{\psi^{n+1} - \psi^n}{\Delta t} = \Lambda_x^{n+1/2}\left(\psi^{n+1} + \psi^n\right) + \Lambda_y^{n+1/2}\left(\psi^{n+1} + \psi^n\right) + f^{n+1/2} \tag{5}$$

The superscript $(n+1)$ refers to the current time and n to the previous one. The operators $\Lambda_x^{n+1/2}$, $\Lambda_y^{n+1/2}$ and $f^{n+1/2}$ are defined as :

$$\Lambda_x^{n+1/2} = \frac{1}{2}\left[-\frac{\partial^4}{\partial x^4} - \frac{k_0^4}{2} - \frac{(\psi^n)^2}{2}\right]; \quad \Lambda_y^{n+1/2} = \frac{1}{2}\left[-\frac{\partial^4}{\partial y^4} - \frac{k_0^4}{2} - \frac{(\psi^n)^2}{2}\right];$$
$$f^{n+1/2} = \frac{1}{2}\left[\epsilon + \frac{g_1}{2}\left(\psi^{n+1} + \psi^n\right) - 2k_0^2\frac{\partial^2}{\partial x^2} - 2k_0^2\frac{\partial^2}{\partial y^2} - 2\frac{\partial^4}{\partial x^2 y^2}\right]\left(\psi^{n+1} + \psi^n\right) \tag{6}$$

2.2 Internal iterations

Since the operators $\Lambda_x^{n+1/2}$, $\Lambda_y^{n+1/2}$ and the function $f^{n+1/2}$ contain terms in the new stage, we do internal iterations. Besides, internal iterations at each time step are required to secure the approximation for the nonlinearities taking part in the scheme of Equation 5.The iterations loop will continue until convergence is attained from monitoring the L_∞ norm. The internal iterations scheme reads :

$$\frac{\psi^{n,p+1} - \psi^n}{\Delta t} = \Lambda_x^{n+1/2}\left(\psi^{n,p+1} + \psi^{n,p}\right) + \Lambda_y^{n+1/2}\left(\psi^{n,p+1} + \psi^{n,p}\right) + f^{n+1/2} \tag{7}$$

where the index (p) refers to the internal iteration number. The superscript $(n, p+1)$ identifies the new iteration, while (n) are the values of the previous time step. The superscript $(n+1)$ for the nonlinear term in the function $f^{n+1/2}$ will be replaced by (n, p), which stands for the values obtained from the previous iteration.

The operators $\Lambda_x^{n+1/2}$, $\Lambda_y^{n+1/2}$ function $f^{n+1/2}$ are redefined as :

$$\Lambda_x^{n+1/2} = \frac{1}{2}\left[-\frac{\partial^4}{\partial x^4} - \frac{k_0^2}{2} - \frac{(\psi^n)^2}{2}\right]; \; \Lambda_y^{n+1/2} = \frac{1}{2}\left[-\frac{\partial^4}{\partial y^4} - \frac{k_0^2}{2} - \frac{(\psi^n)^2}{2}\right];$$
$$f^{n+1/2} = \frac{1}{2}\left[\epsilon + \frac{g_1}{2}\left(\psi^{n,p} + \psi^n\right) - 2k_0^2\frac{\partial^2}{\partial x^2} - 2k_0^2\frac{\partial^2}{\partial y^2} - 2\frac{\partial^4}{\partial x^2 y^2}\right]\left(\psi^{n,p} + \psi^n\right) \tag{8}$$

The iterations proceed until the following criterion for the L_∞ norm is satisfied with $\delta = 1.0 \times 10^{-8}$:

$$L_\infty = \frac{max \mid \psi^{n,p+1} - \psi^{n,p} \mid}{max \mid \psi^{n,p+1} \mid} \leq \delta \tag{9}$$

The last iteration gives the sought function ψ in the new time

$$\psi^{n+1} \stackrel{\text{def}}{=} \psi^{n,p+1} \tag{10}$$

2.3 The splitting scheme

The splitting of Eq. (5) is made according to the Douglas second scheme (also known as scheme of stabilizing correction, shown by Christov *et al.* (1997),Christov and Pontes (2002)). This strategy was chosen to deal with the costly procedure of solving Eq. (7); even though we are dealing with sparse matrices for the operators, the internal iterations makes the process to be repeated several times during each time step. The scheme is designed as follows :

$$\frac{\widetilde{\psi} - \psi^n}{\Delta t} = \Lambda_x^{n+1/2}\widetilde{\psi} + \Lambda_y^{n+1/2}\psi^n + f^{n+1/2} + (\Lambda_x^{n+1/2} + \Lambda_y^{n+1/2})\psi^n \tag{11}$$

$$\frac{\psi^{n,p+1} - \widetilde{\psi}}{\Delta t} = \Lambda_y^{n+1/2}(\psi^{n,p+1} - \psi^n) \tag{12}$$

Here, ψ is the function for the half-time step. In order to show that the splitting represents the original scheme, we rewrite Eqs. (11) and (12) in the form :

$$\left(E - \Delta t\Lambda_x^{n+1/2}\right)\widetilde{\psi} = \left(E + \Delta t\Lambda_x^{n+1/2}\right)\psi^n + 2\Delta t\Lambda_y^{n+1/2}\psi^n + \Delta t f^{n+1/2} \tag{13}$$

$$\left(E - \Delta t\Lambda_y^{n+1/2}\right)\psi^{n,p+1} = \widetilde{\psi} + \Delta t\Lambda_y^{n+1/2}\psi^n \tag{14}$$

where E is the unity operator.

Rearranging these equations, the intermediate variable $\widetilde{\psi}$ is eliminated and the result may be rewritten as :

$$\left(E - \Delta t \Lambda_x^{n+1/2}\right)\left(E - \Delta t \Lambda_y^{n+1/2}\right)\psi^{n,p+1} = \left(E + \Delta t \Lambda_x^{n+1/2}\right)\psi^n + 2\Delta t \Lambda_y^{n+1/2}\psi^n + \\ + \Delta t f^{n+1/2} - \left(E - \Delta t \Lambda_x^{n+1/2}\right)\Delta t \Lambda_y^{n+1/2}\psi^n \tag{15}$$

This result may be rewritten as :

$$\left(E + \Delta t^2 \Lambda_x^{n+1/2}\Lambda_y^{n+1/2}\right)\frac{\psi^{n,p+1} - \psi^n}{\Delta t} = (\Lambda_x^{n+1/2} + \Lambda_y^{n+1/2})(\psi^{n,p+1} + \psi^n) + f^{n+1/2} \tag{16}$$

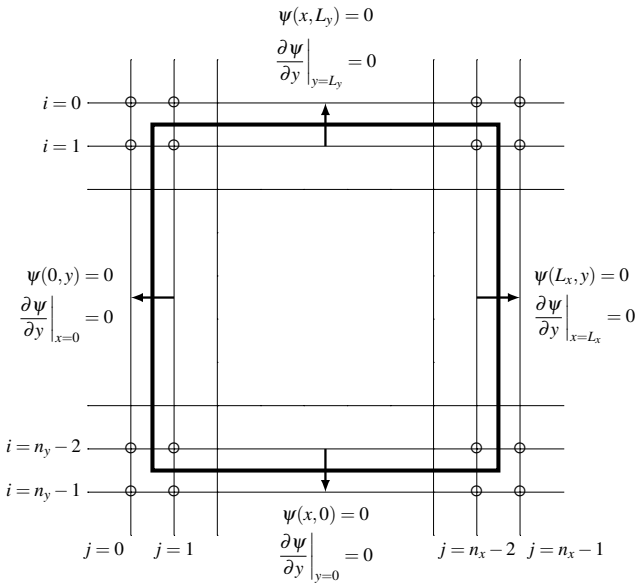

FIGURE 2. The "*Staggered*" grid.

where E is the unity operator. A comparison with Eq. (5) shows that Eq.(16) is actually equivalent to the first one except by the defined positive operator having a norm greater than one :

$$B \equiv E + \Delta t^2 \Lambda_x^{n+1/2}\Lambda_y^{n+1/2} = E + O(\Delta t^2) \tag{17}$$

which acts on the term $(\psi^{n,p+1} - \psi^n)/\Delta t$. This means that this operator does not change the steady state solution. Furthermore, since $||B|| > 1$, the scheme given by eqs. (11)-(12) is more stable than the target one (Eq. (5)).

2.4 Boundary conditions, spatial discretization and the staggered grid

We solve numerically the SH equation with generalized Dirichlet or rigid boundary conditions (GDBC), and periodic (PBC). For the case of rigid boundary conditions we adopt a staggered grid, as represented in Fig. 2. Consider a staggered mesh in both spatial directions, namely

$$x_i = -\frac{\Delta x}{2} + (j-1)\,\Delta x, \quad \Delta x \equiv \frac{L_x}{n_x - 2}, \quad y_i = -\frac{\Delta y}{2} + (i-1)\,\Delta y, \quad \Delta y \equiv \frac{L_y}{n_y - 2},$$

where n_x and n_y are the number of points in x- and y-directions, respectively. The mesh pattern is shown in Fig.2. Let $\psi_{i,j}$ be an arbitrary set function defined on the above described mesh. We confine ourselves to the case of constant coefficients. The PBC, which is less strict than the GDBC, borrows the crystal's structure concept of unit cell, which is representative of a certain volume of the material, allowing us to treat a domain that would also act as a unit cell for a two-dimensional surface, with images being repeated all around the bidimensional domain.

Then the simplest second order symmetric difference approximations of the differential operators are obtained by making a Taylor development of a function ψ in the points of a uniform grid. Considering the function ψ in a bidimensional domain, we can define the derivatives by truncating the Taylor development and arranging the equations. Second derivative with second order accuracy can be written as :

$$\frac{\partial^2 \psi_{i,j}}{\partial x^2} = \frac{\psi_{i,j-1} - 2\psi_{i,j} + \psi_{i,j+1}}{\Delta x^2}; \qquad \frac{\partial^2 \psi_{i,j}}{\partial y^2} = \frac{\psi_{i-1,j} - 2\psi_{i,j} + \psi_{i+1,j}}{\Delta y^2} \tag{18}$$

and the fourth derivative with second order accuracy as :

$$\frac{\partial^4\psi_{i,j}}{\partial x^4} = \frac{\psi_{i,j-2} - 4\psi_{i,j-1} + 6\psi_{i,j} - 4\psi_{i,j+1} + \psi_{i,j+2}}{\Delta x^4}$$
$$\frac{\partial^4\psi_{i,j}}{\partial y^4} = \frac{\psi_{i-2,j} - 4\psi_{i-1,j} + 6\psi_{i,j} - 4\psi_{i+1,j} + \psi_{i+2,j}}{\Delta y^4}$$
$$\frac{\partial^4\psi_{i,j}}{\partial x^2\partial y^2} = \frac{1}{\Delta x^2\Delta y^2}\Big(\psi_{i-1,j-1} - 2\psi_{i,j-1} + \psi_{i+1,j-1} - 2\psi_{i-1,j} + 4\psi_{i,j} - 2\psi_{i+1,j} + \psi_{i-1,j+1} - 2\psi_{i,j+1} + \psi_{i+1,j+1}\Big)$$

On the staggered mesh, all kinds of b.c. are easily approximated with second order approximation, namely

$$\begin{aligned} \psi_{i,0} + \psi_{i,1} &\approx 2\psi\,|_{x=0} \\ \psi_{i,0} - \psi_{i,1} &\approx \Delta x\,\frac{\partial\psi}{\partial x}\Big|_{x=0} \\ \psi_{i,n_x-2} + \psi_{i,n_x-1} &\approx 2\psi\,|_{x=L_x} \\ -\psi_{i,n_x-2} + \psi_{i,n_x-1} &\approx \Delta x\,\frac{\partial\psi}{\partial x}\Big|_{y=L_y} \\ \text{for } i = 2, ..., n_y - 3 & \end{aligned} \qquad \begin{aligned} \psi_{0,j} + \psi_{1,j} &\approx 2\psi\,|_{y=0} \\ -\psi_{0,j} + \psi_{1,j} &\approx \Delta y\,\frac{\partial\psi}{\partial x}\Big|_{y=0} \\ \psi_{n_y-2,j} + \psi_{n_y-1,j} &\approx 2\psi\,|_{x=L_x} \\ -\psi_{n_y-2,j} + \psi_{N-1,j} &\approx \Delta y\,\frac{\partial\psi}{\partial x}\Big|_{y=L_y} \\ \text{for } j = 2, ..., n_x - 3 & \end{aligned}$$

Hence, the approximations of the Dirichlet b.c. of the first kind read

$$\begin{aligned} \psi_{i,0} &= \psi_{i,1} = 0 \qquad \psi_{i,n_x-1} = \psi_{i,n_x-2} = 0 \\ \psi_{0,j} &= \psi_{1,j} = 0 \qquad \psi_{n_y-2,j} = \psi_{n_y-1,j} = 0. \end{aligned} \tag{19}$$

We adopt the generalized Dirichlet boundary condition (function value and first derivative equals zero).

3. SCHEME STABILITY

One important issue which concerns the simulations is the time and mesh size selection, such that we seek reasonable choices inside the stable region of the present semi-implicit scheme. Here, we study the time step variation effect regarding the structure evolution assessing the rate of change in time of the pattern during the simulation by monitoring the relative L_1 norm defined as :

$$L_1 = \frac{1}{\Delta t}\frac{\sum_{i,j} |\,\psi^{n+1} - \psi^n\,|}{\sum_{i,j} |\,\psi^{n+1}\,|} \tag{20}$$

which roughly corresponds to the ratio between the spatial average of the modulus of time derivative $\partial\psi/\partial t$ and the spatial average of the modulus of the function itself. The calculations begin from a random initial condition and proceeded until $L_1 \leq 1 \times 10^{-6}$, when it can be assumed that the state is steady. Following this implementation, Figure 3 shows the structure evolution through the L_1 parameter to observe when the results would diverge for an increasing time step Δt.

An interesting result was attained for $\Delta t = 2.0$ (not exposed). In this case, a distinct steady state (spurious solution) was reached, leading us to believe that the operator splitting method do not deal well with high Δt values, but provides the same solution for sufficiently large Δt when compared to explicit methods. This is an advantage that enables reaching the desired numerical solutions with lower computational time. A conservative choice for all simulations would be $\Delta t = 0.1$, which presents the same results as for $\Delta t = 0.01$. However, the choice was $\Delta t = 0.5$ so that lower computational time is required without losing physically consistent results given stability.

4. NUMERICAL RESULTS

The numerical scheme above described was used to solve the SH equation in square domains with rigid and periodic boundary conditions, and a variable control parameter across the domain. The parameter values adopted are given in Table 1. All simulations were run starting from the same random initial condition. In addition to the parameters given in the table, we assumed $k_0 = 1.0$ and $\Delta t = 0.5$. All simulations presented were done in a rather coarse spatial grid, consisting of 16 points per critical wavelength (*mesh*). The results of ten simulations are presented, five of them assuming rigid (generalized Dirichlet) boundary conditions, and the remaining five, with periodic boundary conditions. The steady state solution obtained are shown in Fig. 4. The first line in this figure shows the distribution of the control parameter

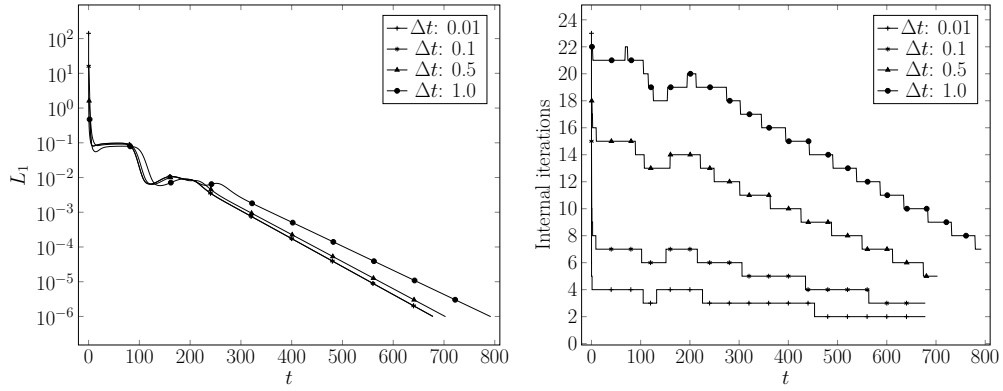

(a) (b)

FIGURE 3. Stability analysis from the numerical integration of the Swift-Hohenberg equation. (a) L_1 norm and (b) internal iterations are shown as a function of time t for a 64×64 nodes domain. The same steady pattern is reached for each time step at the end of the simulations from the same random initial conditions.

along the x-direction of the domain. In all cases, the parameter is assumed as uniform along the y-direction. Second and fourth lines present the steady state solutions with rigid and with periodic boundary conditions, respectively. Third an fifth lines present the same results shown in lines two and four, but the frames were constructed with enhanced contrast to make visible the subcritical structure developed in regions where the control parameter assume negative values. Each configuration run is identified with an assigned number.

TABLE 1. Parameters assumed for the simulations presented in this work

Parameter	Formulæ	Value	Description
k_0	-	1.0	critical wavenumber
λ_0	$2\pi/k_0$	2π	critical wavelength
g_1	-	0.0	coefficient of symmetry breaking
w_x, w_y	-	10	wavelengths per domain side
n_{w_x}, n_{w_y}	-	16	nodes per wavelength (resolution)
n_x, n_y	$w_x n_{w_x}$,$w_y n_{w_y}$	160	nodes per mesh side (n)
L_x, L_y	$w_x\lambda_0$, $w_y\lambda_0$	≈ 62.8319	domain side (L)
Δx,Δy	$L/(n-2)$	≈ 0.3977	space step (GDBC)
Δx,Δy	L/n	≈ 0.3927	space step (PBC)
Δt	-	0.5	time step

Configurations 1 shows the well known result of a system uniformly forced and rigid boundary conditions. The case was run in the framework of validating our numerical code. A pattern with unavoidable defects is developed, in order to match the strong requirement of rolls approaching perpendicularly the side walls. A structure with lower density of defects appears in Configuration 6, where the same forcing of Frames 1 is assumed, but now, with periodic boundary conditions. The pattern develops a zig-zag instability.

Configurations 2 also present the well know result of a pattern developed in presence of a ramped control parameter, with a subcritical control parameter. A structure with smaller amount of defects emerges, thanks to the fact that the weak structure of rolls parallel to the wall appears in the subcritical region. A similar situation occurs in Configuration 3, where the system is forced with a ramp of the control parameter, however taking non negative values. In this case an weak structure of rolls perpendicular to the lower $(y = 0)$ sidewall is visible.

Configurations 7 and 8 present the results for systems with same forcing of configurations 2 and 3, but with [periodic boundary conditions. A tendency to develop a structure of rolls parallel to the gradient of the control parameter clearly appears, as well as the existence of a Benjamin-Feir instability close to the left wall, induced by the the supercritical region close to the right wall.

Configurations 4, 5, 9 and 10 present the result of simulations performed with a Gaussian distribution of the control parameter, the former two with rigid boundary conditions and latter ones, with periodic conditions. A thiner Gaussian, rapidly decreasing from the maximum value across a short distance leads to the onset of a target pattern with both boundary conditions. The target collapses in presence of a wider Gaussian distribution of the control parameter, leading to a structure of rolls. The structure wavevector takes the direction of one of the domain diagonals, again, in consequence of the property

that the most difficult direction for modulations of the modulation of the structure is the one associated to the wavevector, whereas the easiest one is the direction perpendicular to the wavevector.

The velocity of evolution of the ten simulations presented in Fig. 4, captured by the rate of change of the L_1 norm is shown in Fig. 5. All curves show the well known result that L_1 rapidly decreases as a pattern emerges and the amplitude of the structure essentially saturates. This phase is followed by a much slower phase dynamics with a clear nonlinear evolution. Defects are removed, when L_1 accelerates, as a rule. The evolution end at a third phase, ending with an exponential decay.

The evolution of Configurations 3, 4 and 7, from the random initial condition to the steady state in shown in Figure 6, 7 and 8. We implemented the gradient of the control parameter in all directions with a Gaussian distribution of the control parameter with the maximum in the center of the system, according to :

$$\epsilon(x, y) = 0.2e^{-R((x-x_0)^2+(y-y_0)^2)} \tag{21}$$

where $n = n_x = n_y$; $R = n^3$ for configurations 4 and 9, while $R = 0.2\, n^3$ for configurations 5 and 10.

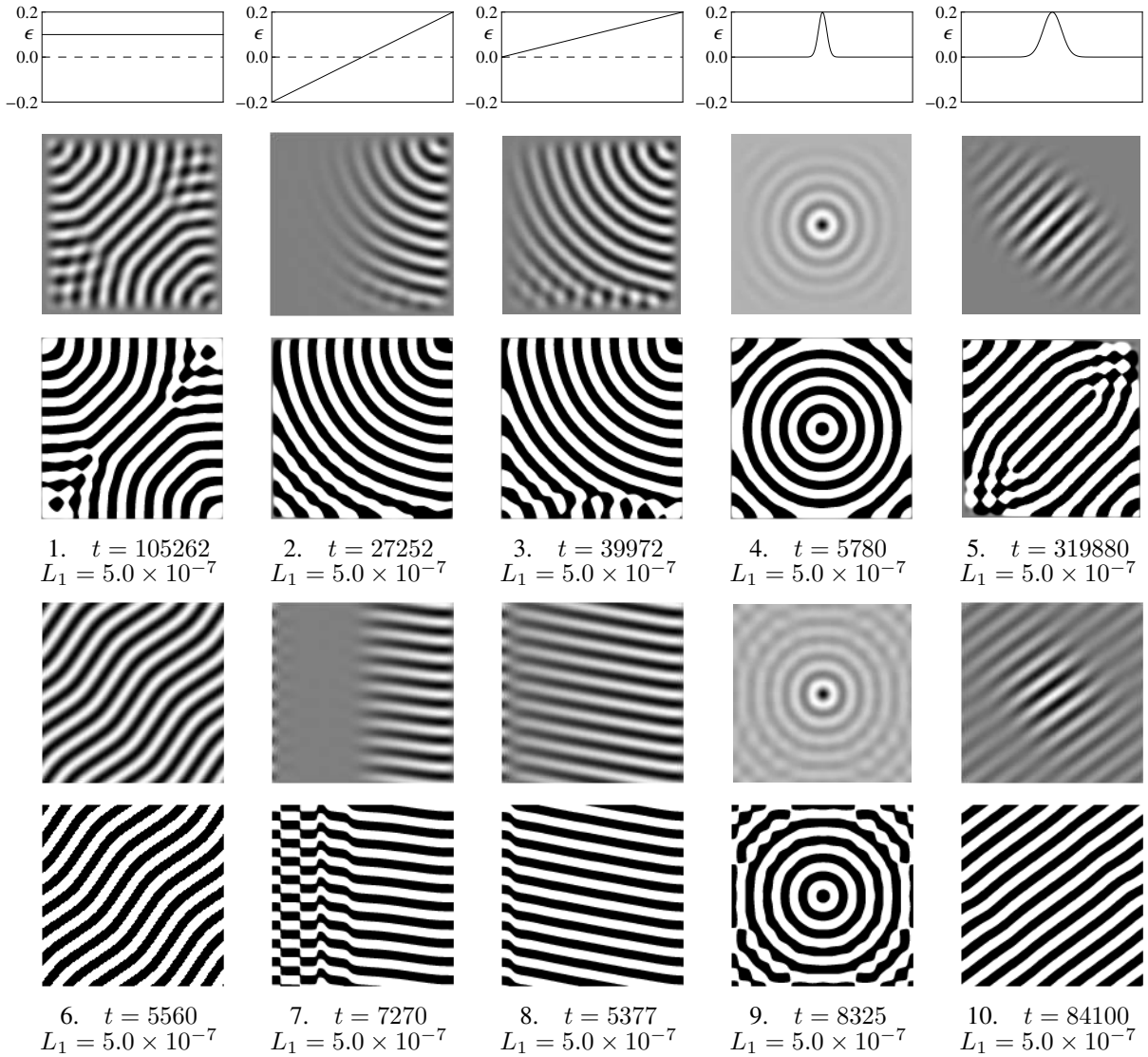

FIGURE 4. Structures obtained numerically from the Swift-Hohenberg equation for subcritical and supercritical values of ϵ and $\epsilon = 0.1$. The variation of the bifurcation parameter across the domain is represented on the top of each diagram. The first and third rows corresponds to generalized Dirichlet boundary conditions and periodic boundary conditions, respectively. Second and fourth rows contains the same patterns from above with an enhanced contrast.

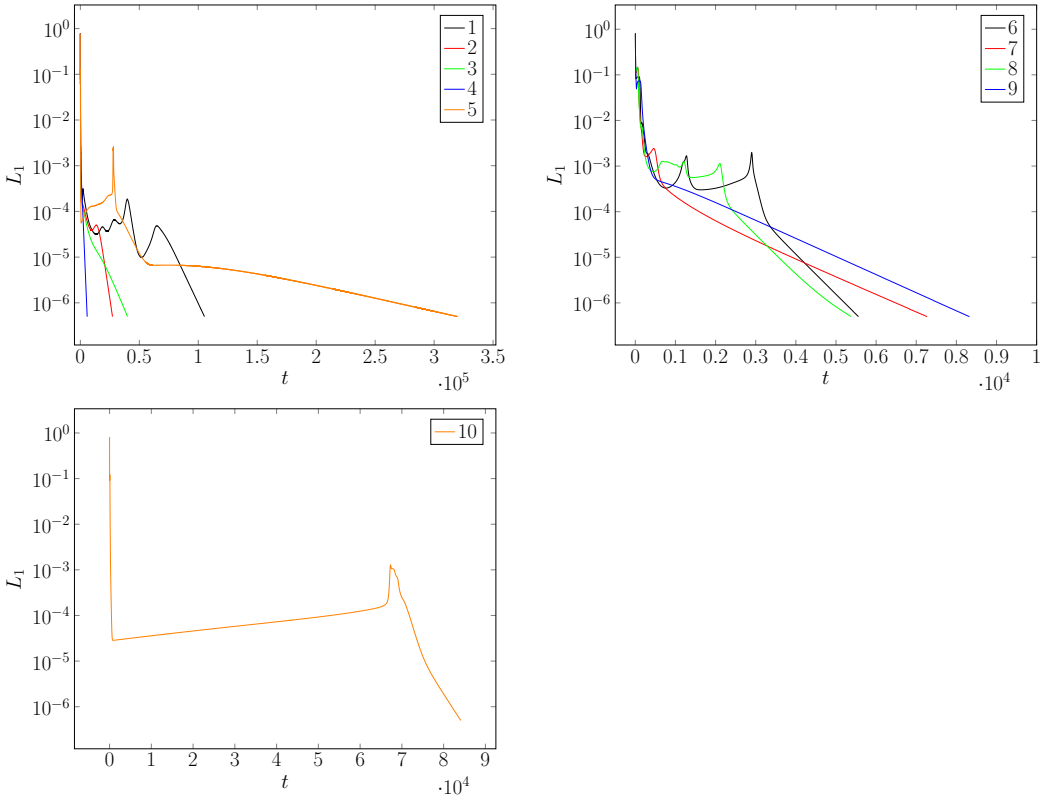

FIGURE 5. Evolution of the rate of change of the distance between two successive system states, as captured by L_1. The curves are identified with the number associated to each configurtation run.

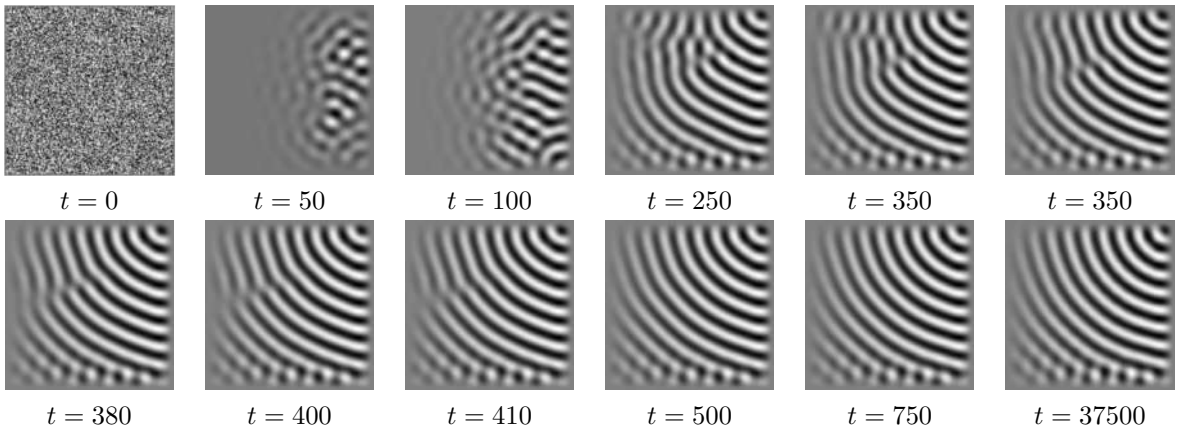

FIGURE 6. Pattern evolution for the configuration 3 until the steady state.

5. CONCLUSION

In the present endeavour, we investigated pattern formation by means of numerical integration of the Swift-Hohenberg equation in two dimensions and with nonuniform distributions of the control parameter. All simulations were started from the same random initial conditions at $t = 0$. Distinct boundary conditions were assumed, i.e., rigid (GDBC) and periodic (PBC) for all control parameter set-ups. The PBC was implemented in order to capture a less restrict dynamics, in which fewer defects for the steady states can be seen. This type of boundary conditions maintain the domain properties and provide significant complementing results to the ones found in the literature.

In the literature, simulations with a uniform control parameter are well known for both boundary conditions tested. A ramped control parameter mostly appear in the sense of rigid boundaries. Using periodic boundary conditions for the latter case resulted in structures with the Benjamin-Feir instability, which manifest itself in the form of “alternating” rolls, in a dislocation sense, promoted by a region where minimum and maximum values of ϵ are close. Configurations 6-10 (PBC) are free from rigid boundaries and thus are only subjected to the nonuniform forcing from the same random initial conditions.

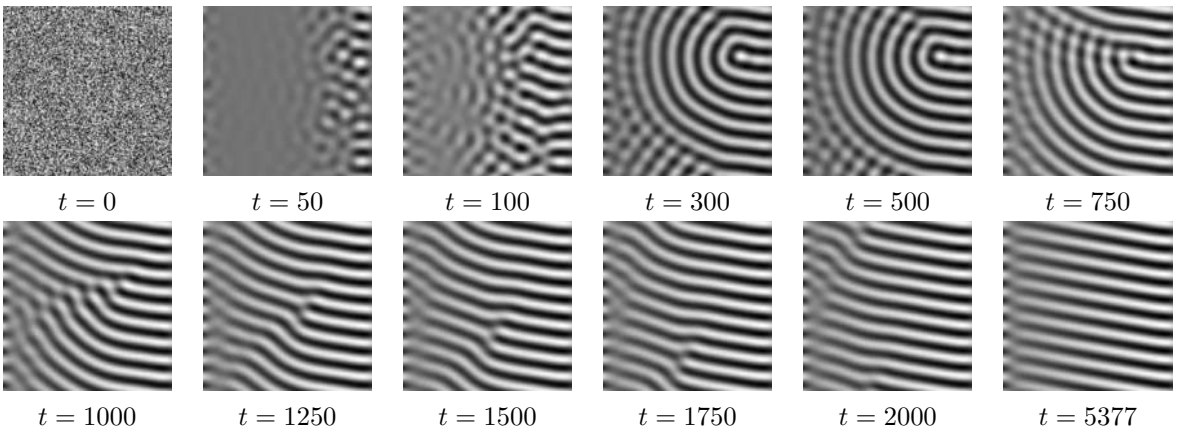

FIGURE 7. Pattern evolution for the configuration 8 until the steady state.

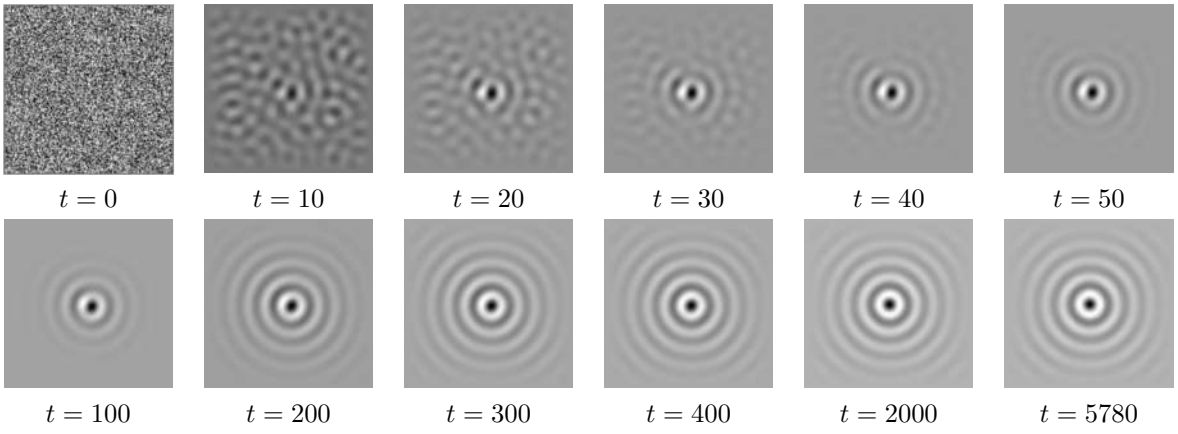

FIGURE 8. Pattern evolution for the configuration 4 until the steady state.

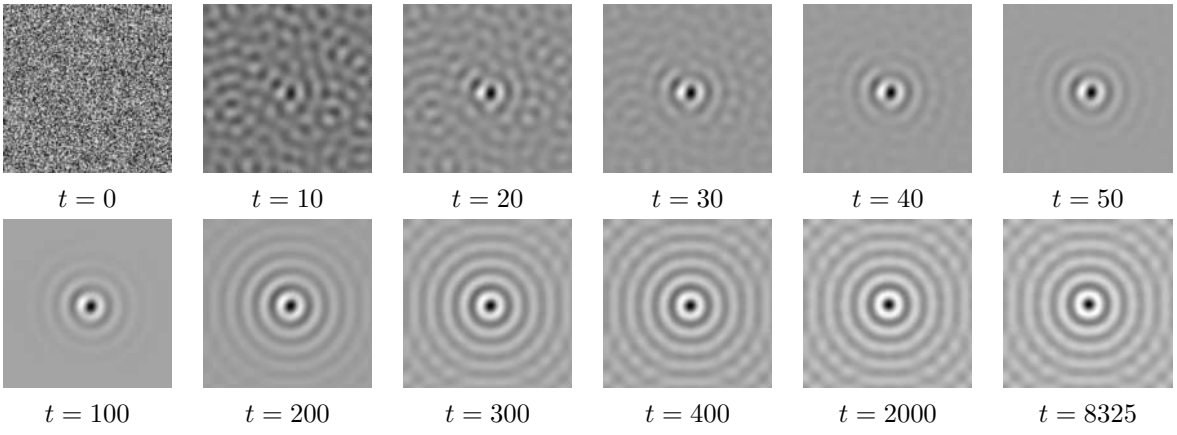

FIGURE 9. Pattern evolution for the configuration 9 until the steady state.

The developed finite-difference time splitting scheme was proven to be unconditionally stable. This numerical scheme and algorithm were implemented following successful endeavours in the literature (Christov *et al.* (1997); Christov and Pontes (2002); Vitral *et al.* (2018); Pontes *et al.* (2008)). The attempt to attain the pattern zoology for the nonuniformly forced Swift-Hohenberg equation (with ramped and Gaussian distributions for ϵ) was successful and further theoretical and numerical investigations are required. Future work will involve a more robust code verification (convergence analysis), numerical set-ups with more choices of the control parameter distributions and a lot more simulations.

6. ACKNOWLEDGEMENTS

The authors would like to thank the support from CNPq, FAPERJ and CAPES.

7. REFERENCES

Boyer, D. and Viñals, J., 2002. "Grain boundary pinning and glassy dynamics in stripe phases". *Physical Review E*, Vol. 65.

Christov, C. and Pontes, J., 2002. "Numerical scheme for swift-hohenberg equation with strict implementation of lyapunov functional". *Mathematical and Computer Modelling*, Vol. 35.

Christov, C., Pontes, J., Walgraef, D. and Velarde, M., 1997. "Implicit time splitting for fourth-order parabolic equations". *Computer Methods in Applied Mechanics and Engineering*, Vol. 148.

Cross, M.; Hohenberg, P., 1993. "Pattern formation outside of equilibrium". *Review of Modern Physics*, Vol. 65.

Douglas, J. and Rachford., H.H., 1956. *On the numerical solution of heat conduction problems in two and three space variables*. Trans. Amer. Math. Soc. ISBN 82 :421-439.

Haken, H., 1983. *Synergetics*. Springer–Verlag, Berlin.

Haken, H., 1993. *Advanced Synergetics*. Springer–Verlag, Berlin.

Pontes, J. and Mangiavacchi, N., 2016. *Fenômenos de Transferência com Aplicações Ciências Físicas e a Engenharia – Volume 1 : Fundamentos*. SBM – Sociedade Brasileira de Matemca. ISBN 978-85-8337-107-6.

Pontes, J., Mangiavacchi, N., Alves, L.S.B., Anjos, G., Eto-Hiroms, K. and Hirata, S., 2018. *Fenômenos de Transferência com Aplicações Ciências Físicas e a Engenharia – Volume 2 : Aplicações*. SBM – Sociedade Brasileira de Matemática. ISBN 978-85-8337-153-3.

Pontes, J., Walgraef, D. and Christov, C.I., 2008. "Pattern formation in spatially ramped rayleigh-bénard systems". *Journal of Computational Interdisciplinary Sciences*, Vol. 1, No. 1, pp. 11–32.

Provatas, N. and Elder, K., 2010. *Phase-Field Methods in Materials Science and Engineering*. Wiley. ISBN 3527407472,9783527407477.

Swift, J. and Hohenberg, P.C., 1977. "Hydrodynamic fluctuations at the convective instability". *Physical Review A*, Vol. 15.

Vitral, E., Walgraef, D., Pontes, J., Anjos, G. and Mangiavacchi, N., 2018. "Nano-patterning of surfaces by ion sputtering : Numerical study of the anisotropic damped kuramoto-sivashinsky equation". *Computational Materials Science*, Vol. 146.

Viñals, J., 2009. "Defect dynamics in mesophases". *Journal of the Physical Society of Japan*, Vol. 78, No. 4, pp. 041011–041011.

Walgraef, D., 1997. *Spatio-Temporal Pattern Formation : With Examples from Physics, Chemistry, and Materials Science*. Partially Ordered Systems. Springer-Verlag New York, 1st edition. ISBN 978-1-4612-7311-0,978-1-4612-1850-0.

Walgraef, D. and Aifantis, E.C., 1985. "Dislocation patterning in fatigued metals as a result of dynamical instabilities". *Journal of Applied Physics*, Vol. 58.

Walgraef, D., 1987. "Patterns, defects and microstructures in nonequilibrium systems : Applications in materials sciences ; proceedings of the nato advanced research workshop, university of texas, austin, mar. 24-28, 1986". In *Workshop organised by the University of Texas and Universite Libre de Bruxelles ; Supported by NATO and NSF. Dordrecht, Martinus Nijhoff Publishers (NATO ASI Series, No. E121), 1987, 395 p. No individual items are abstracted in this volume.* Vol. 121.

Walton, I., 1982. "On the onset of rayleigh-bénard convection in a fluid layer of slowly increasing depth". *Studies in Applied Mathematics*, Vol. 67, No. 3, pp. 199–216.

Walton, I., 1983. "The onset of cellular convection in a shallow two-dimensional container of fluid heated non-uniformly from below". *Journal of Fluid Mechanics*, Vol. 131, pp. 455–470.

Yanenko, N.N. and Holt, M., 1971. *The Method of Fractional Steps*. Springer. ISBN 3540052720, 9783540052722.

8. RESPONSIBILITY NOTICE

The authors are the only responsible for the printed material included in this paper.